Anodic Cu_2S and CuS Nanorod and Nanowall Arrays: Preparation, Properties and Application in CO_2 Photoreduction

Piyush Kar,[1]* Samira Farsinezhad,[1] Xiaojiang Zhang[1] and Karthik Shankar[1,2]*

[1]Department of Electrical and Computer Engineering, University of Alberta,
9107 - 116 St, Edmonton, Alberta, Canada T6G 2V4

[2]National Institute for Nanotechnology, National Research Council, 11421 Saskatchewan Dr, Edmonton, AB, Canada T6G 2M9

*** Authors to whom all correspondence must addressed:**

1. Piyush Kar, pkar1@ualberta.ca
2. Karthik Shankar, kshankar@ualberta.ca

ABSTRACT

Copper sulfide semiconductors made from earth-abundant elements have an optical absorption edge at *ca.* 1.2 eV, nearly ideal for solar energy harvesting. We report the growth and formation mechanism of vertically oriented arrays of copper sulfide nanostructures formed by electrochemical anodization. Key parameters that affect the morphology and phase of the nanostructures are type and strength of electrolyte, anodization voltage and duration. Cu_2S and CuS nanostructures were obtained on both copper foil and copper-coated flexible Kapton substrates, and depending on the anodization parameters, consisted of vertically oriented arrays of nanowalls, nanoleafs or rods with branched nanodendrites. The anodization parameters also controlled the phase and stoichiometry of the nanostructures. *p*-type conduction for Cu_2S

nanostructures and *n*-type conduction for CuS nanostructures were revealed by admittance spectroscopy and Mott Schottky analysis. We also observed a weak, but nevertheless promising and previously unnoticed, photocatalytic action in copper sulfide nanorod and platelet arrays for the sunlight-driven conversion of CO_2 into CH_4. Under irradiation by AM 1.5G simulated sunlight at room temperature, a CH_4 production rate as high as 38 μmol m^{-2} h^{-1} was obtained using the copper sulfide nanostructure arrays as stand-alone photocatalysts for CO_2 photoreduction.

KEYWORDS

Cu_2S; CuS;dendritic nanostructures; alpha-chalcocite; covellite;electrochemical anodization; methanation; solar fuels; reduction; semiconductor photocatalysis; electrochemical impedance spectroscopy; charge carriers;

1 Introduction

As grown Cu_2S and CuS are degenerate semiconductors with a thin film carrier mobility of 1-6 cm^2/V-s, at room temperature.[1-4] While 1.2 eV is the most frequently reported location for the Cu_2S band-edge, band-edges up to 1.4 eV are observed due to the degenerate doping-induced Moss-Burstein shift.[5] Both direct and indirect transitions have been reported for Cu_2S[6] although its high absorption coefficient of 1-8 x 10^4 cm^{-1} over the 400-1000 nm spectral range points to a direct bandgap,[7] strongly supported by recent electronic structure calculations.[8, 9] The low band-gap and high absorption coefficient of Cu_2S are nearly ideal for optimal absorption of sunlight. $Cu_{2-x}S$ has also been shown recently to exhibit localized surface plasmon resonance (LSPR) at near-infrared wavelengths originating in the light-induced stimulation of the collective

oscillations of the large carrier population.[10] The ability of nanostructured copper chalcogenides to simultaneously exhibit excitonic and plasmonic resonances makes them a unique platform for the study of exciton-plasmon interactions.[11] CuS has a direct band-gap of 2.0 eV and although reported to be semiconducting in amorphous form, exhibits metallic conduction[12, 13] in crystalline and polycrystalline forms. Recently, CuS has been shown to be a good reductive co-catalyst on supports such as ZnS and ZnO,[14, 15] due to its relatively small electron affinity and the consequent high reducing power of its conduction band electrons. There has also been a resumption of interest in CuS as an unconventional superconductor.[16, 17] Copper sulfides have potential applications in photovoltaics,[18-20] photocatalytic water-splitting,[21] field emitters,[22] non-volatile memories,[23] biosensors,[24] optical limiters,[25] photothermal cancer cell ablation[26] and lithium ion batteries[27, 28] due to favorable optical, electrical and superionic properties. Copper deficiency and nanostructured morphology render adjustable band-gaps of the *p*-type Cu_2S semiconductor materials between 1.2 and 2.0 eV, and therefore enable tunable properties. Here, we report the controlled synthesis and thorough characterization of oriented arrays of copper sulfide nanostructures. Another unique feature of our work is our observation of the activity of copper sulfide nanostructures as catalysts for the reduction of CO_2 to methane.

Electrochemical anodization is a simple, low cost and high-throughput method currently used to generate arrays of vertically oriented, self-organized nanopores and nanotubes in a variety of valve metal oxides including, but not limited to, Al_2O_3, TiO_2, Nb_2O_5, Ta_2O_5, Fe_2O_3, WO_3, ZrO_2 and HfO_2.[29] Key advantages of anodization include the availability of multiple process variables such as the temperature, duration, electrolyte composition, anodization potential (or current), anodization ramp (or pulse) sequence and substrate patterning, to control the rates of competing processes and thereby obtain a tunable and reproducible morphology at

the nanoscale. Anodization has not been hitherto employed for the growth of vertically oriented nanostructures in copper sulfide. The minority carrier recombination diffusion length (L_h) in monocrystalline chalcocite is 30-35 nm[30] thus motivating the formation of nanostructures of sizes comparable to L_h in order to ensure efficient separation of photogenerated charges. Existing reports on copper sulfide nanostructure growth are limited to nanoparticles,[10, 20] thin films[6, 31-34] and nanowires.[35] Nanowire formation is based on template[36-38] and diverse chemical methods.[39-41] Drawbacks of the existing methods include high cost, aggressive and high temperature environment, and poor control over process and nanostructure morphology. Nanostructure morphology significantly affects functionality, and can be controlled by the various parameters of the electrochemical anodization process as pointed out above.

2 Experimental

2.1 Synthesis of nanostructured copper sulfides

Copper substrates were first cleaned with 1% HCl to remove a thin layer of native oxide on the surface. Cu_2S and CuS nanowall, nanoleaf and nanorod arrays were grown by the potentiostatic anodization of copper at voltages between 1.5 and 8 V in an electrolyte which consisted of an aqueous solution of 0.05-1.5 M sodium sulfide. Concurrently, planar films of copper sulfide were grown by immersing copper substrates in aqueous 0.02 M Na_2S while a bias voltage of -0.3V was applied at the anode for various time spans. For both planar and nanostructured films, subsequent to the completion of anodization, the substrates were taken out of the aqueous bath and left alone to dry in air without any cleaning or drying steps. Two types of Cu substrates were anodized - copper foils and copper thin films deposited on commercially

available polyimide (Kapton®) substrates. Cu foils were obtained from Fisher Scientific (USA), and substrates of size 2 cm x 4 cm x 0.0125 cm were used for anodization. In addition, 1 µm thick Cu films were formed by DC Magnetron Sputtering at 300 W and 7 x 10^{-3}Torr on to 50 µm-thick Kapton substrates of size 1 cm x 4 cm. Anodization was performed at two different temperatures: room temperature and also at 5 °C. Ti foils (obtained from Alfa Aesar, USA) were used as cathode and were 0.5 cm x 4 cm x 0.089 cm in dimension. Three-fourths of the sample area, for both foil and Kapton substrates, was immersed in the electrolyte during the anodization process. Distance between anode and cathode were maintained at approximately 3 cm. Anodization time was controlled such that the process could be terminated at a short time of 15 seconds and while also allowing for longer durations.

2.2 Characterization

Scanning electron micrographs of the morphology of the samples were collected using both a Hitachi S-4800 field-emitter-based instrument and a Zeiss LEO 1430 hot-cathode based instrument. X-ray diffractograms of the samples were collected using a Rigaku Ultimate IV multipurpose XRD system. X-ray photoelectron spectroscopy was performed using an Axis Ultra spectrometer from Kratos Analytical. Transmission electron microscopy (TEM) was performed using a JEOL 2200 FS TEM at an acceleration voltage of 200 kV.

2.3 CO_2 photoreduction

The experimental setup for the photocatalytic reduction test is shown in Fig. 1. As-anodized copper sulfide samples (2 cm wide, 2 cm long) were placed in a stainless steel reaction chamber with water droplets (5 µL, 1 mm diameter). A Newport solar simulator was employed as the light source to irradiate AM 1.5 sunlight to the samples. Before further experiments, the

chamber was first purged with 1% CO_2 (balance = nitrogen) and then filled with 5.5 atm. 1% CO_2. The photoreduction of CO_2 with water was carried out at room temperature. Duration of exposure to simulated solar light was maintained at one hour. The products were identified using a Poropak QS column in a Varian Star gas chromatograph (GC) equipped with a flame ionization detector (FID) and a thermal conductivity detector (TCD).

2.4 Electrochemical impedance spectroscopy

Samples for electrochemical impedance spectroscopy (EIS) were prepared by taking as-synthesized nanostructured copper sulfide grown on copper foils and covering all parts of the samples with parafilm but keeping a 1 cm^2 section on each sample surface exposed to electrolyte. EIS was conducted in a 0.1 M phosphate buffer solution (PBS) and with a Ag/AgCl reference electrode and platinum counter electrode in the frequency range of 1 to 10^6 Hz. The potential window for acquiring EIS data was maintained near the open circuit potential of copper sulfide, as reported in the literature.[42]

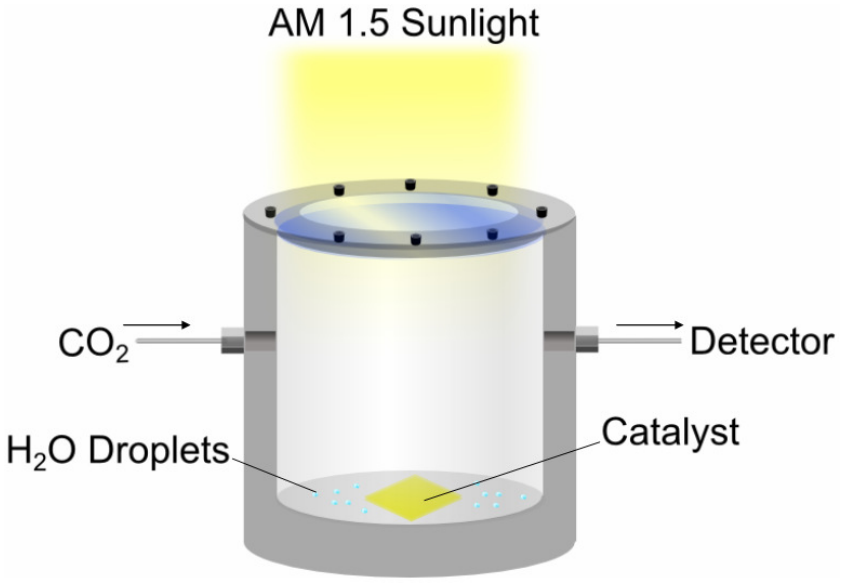

Fig. 1 Schematic of experimental setup for our photocatalytic CO_2 reduction tests. Copper sulfide films of different morphologies (as indicated in Table 1) were tested for performance in photocatalytic CO_2 reduction.

3 Results and Discussion

Vertically oriented copper sulfide nanostructures were formed by the potentiostatic anodization of copper foil in aqueous solutions of sodium sulfide at voltages between 1.5 and 8 V. The concentration of Na_2S was varied between 0.05 M and 1.5 M depending on the applied anodization voltage, which was experimentally determined as appropriate. As a rule, higher concentrations were required for higher anodization voltages. Lower concentrations tended to slow down the formation of the compact sulfides delaying the nanostructure formation process. At higher Na_2S concentrations, copper sulfide formation kinetics are rapid leading to a thick compact layer, the potential drop across which in turn decreases the effective anodization voltage slowing down the field-induced migration of Cu^+ ions to the Cu_2S-electrolyte interface resulting in deceleration and/or inhibition of vertically oriented nanostructure formation.

3.1 Morphology of copper sulfide nanostructures formed at various voltages and temperatures

At room temperature, a Na_2S concentration of 0.1 M and an anodization voltage of 1.5 V, the morphology of anodized Cu foils consisted of vertically oriented, curled plate-like structures as shown in Figs. 2a and 2c. When the anodization was conducted at a lower temperature of 5°C and at a voltage of 3 V, the morphology (shown in Fig. 2b) still consisted of nanowalls, which were however not curled and were also thicker in width than the curled nanowalls in Fig. 2c. The high magnification top-view image in Fig. 2b indicates the width of the walls to be 50 nm. Cross-sectional SEM images, such as the one shown in Fig.S1 in Supporting Information, show

the nanowalls to be approximately 4 µm in height and oriented vertically to the underlying copper substrate. To determine whether the uncurled nanowall structure is produced by the higher voltage or lower temperature, we conducted the same anodization process on a Cu foil sample at 1.5 V and 5°C. The resulting sample once again consisted of curled walls (Fig. 2d), indicating that the anodization voltage played a more prominent part than temperature in determining the morphology of anodic copper sulfide nanostructures.

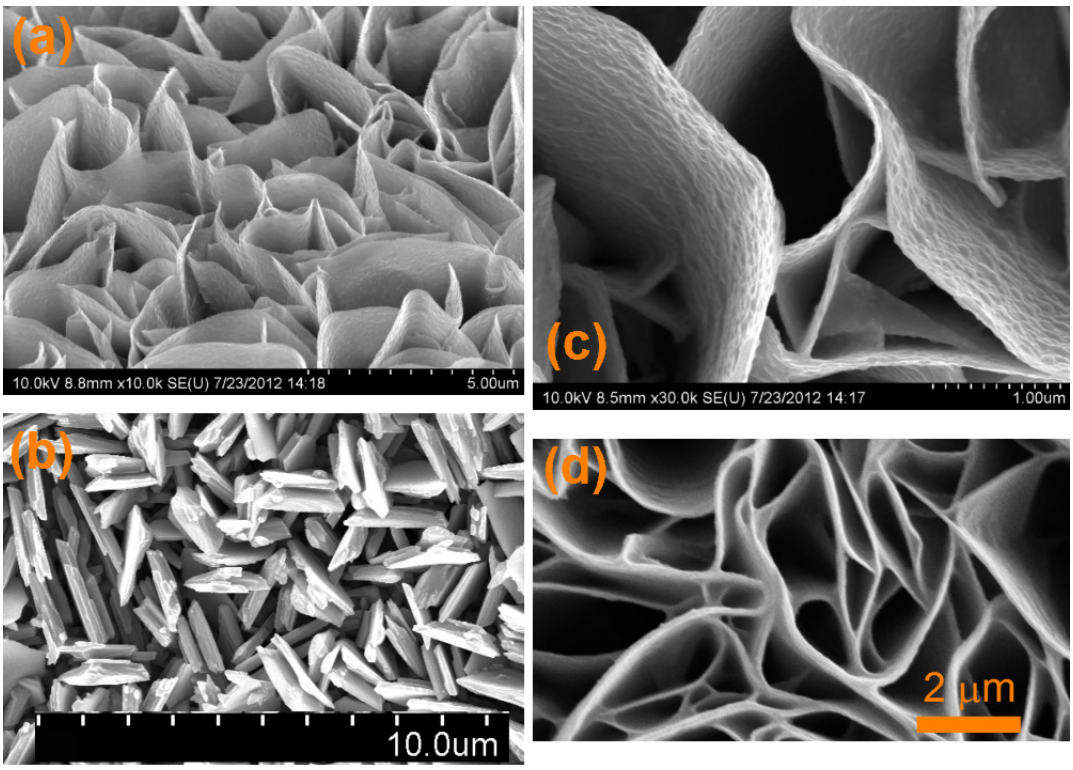

Fig. 2 FESEM images of the morphology of copper sulfide nanowalls oriented vertical to the substrate formed by anodization of copper foil in aqueous Na_2S electrolyte at low voltage and/or low temperature. a) 1.5 V at room temperature (profile view) b) 3 V at 5°C (top-view) c) 1.5 V at room temperature (top-view) and d) 1.5 V at 5°C (top-view).

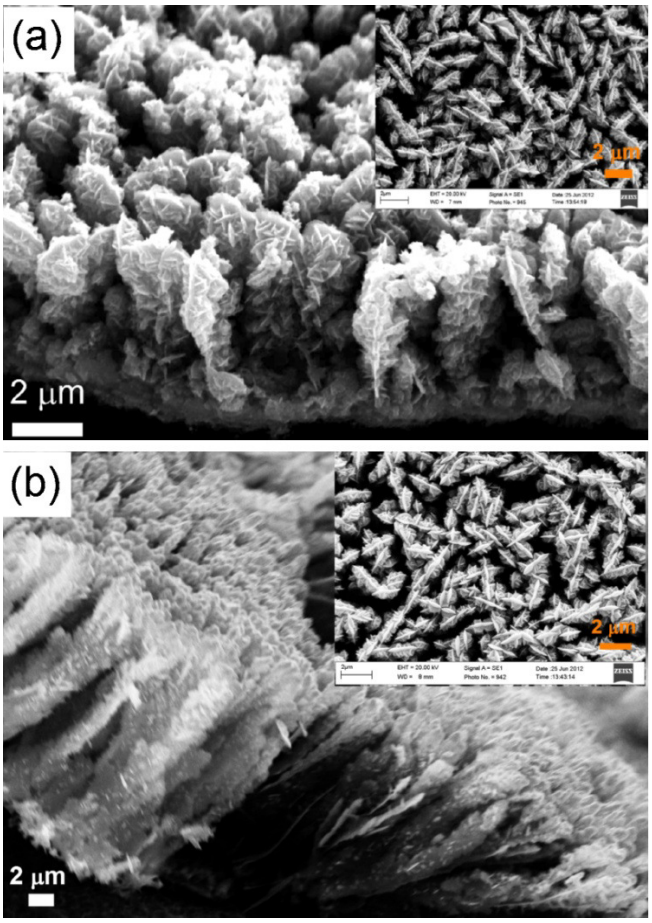

Fig. 3 SEM images of the cross-section of vertically oriented copper sulfide nanorod arrays on copper foil formed anodically at room temperature at a) 3 V and b) 4 V. In both (a) and (b), the insets show top-views indicative of dendritic tips, but only the 3V sample also has a branched cross-section.

When copper foils are anodized at room temperature at voltages higher than 2 V, the morphology of the copper sulfide nanostructures changes from nanowalls to regular and branched rods with dendritic tips as shown in Fig. 3. When high anodization voltages are applied at a temperature of 5ºC, nanowalls with dendritic protrusions along the walls (nanoleaf structures) are obtained as in Fig. 4. Figs. 4a and 4b show the top view of nanoleaf like Cu_2S

structures formed by anodization at 4 and 8 V respectively, which are formed at 5°C by anodization in 0.1 M Na_2S electrolyte. Both Figs. 3 and 4 indicate that the tendency to form nanowall-like structures is dominant at low temperatures, and competes with a tendency to form dendrites at higher anodization voltages. When both high voltages and low temperature are applied, nanoleaves are obtained. The behaviour of the sample anodized at 3V provides insight into the evolution of the nanostructure morphology with anodization time. Curled and straight nanowalls (Figs. S1a and S1b, Supporting Information) are prevalent in the initial stages of anodization. With increase in anodization time, these wall-like structures grow taller and become rods bearing dendritic nano-branches, as shown Fig. S1c.

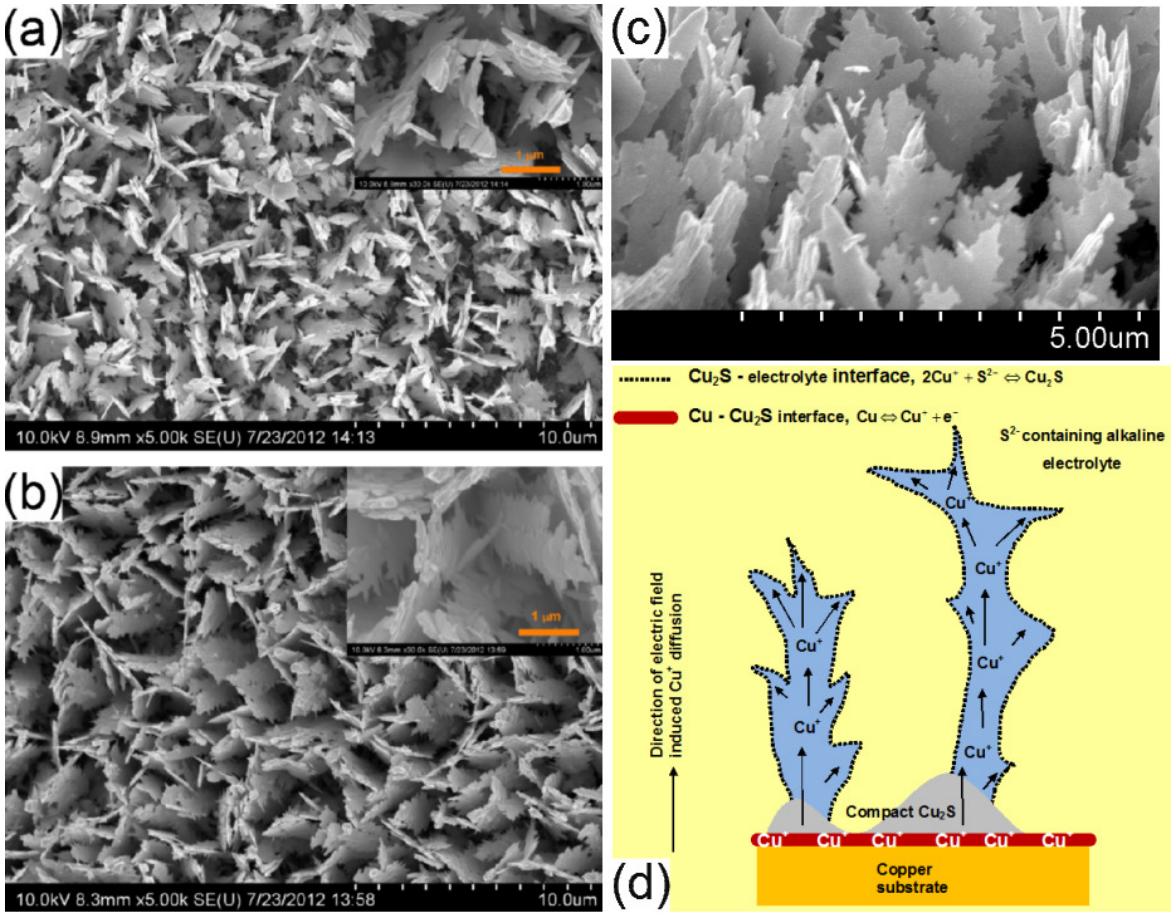

Fig. 4. (a) and (b) show SEM micrographs of vertically oriented dendritic nanowall structures formed by anodization of copper foils at 5ºC at 4 V and 8 V respectively. Insets are magnified top views showing individual dendrites;(c) is an SEM profile view of the 8 V sample and (d) is a schematic explaining the mechanism of vertically oriented growth of copper sulfide nanostructures.

3.2 Growth mechanism of anodized copper sulfide nanostructures

Copper readily forms sulfide products upon exposure to sulfide containing solutions, and as a result of introduction of copper into aqueous sulfide solution, a compact sulfide layer forms spontaneously on the surface of the copper substrate.The electrochemical oxidation of copper in aqueous sulfide solutions consists of three steps[43, 44] : (i) The formation of HS^-, S^{2-}, $OH^-$and O^{2-} anions by the field-induced dissociation of sulfide species, water and hydroxyl ions, respectively, which is followed by their diffusion to the surface of the anode(ii) The dehydration of these anions prior to entry into the electrical double layer and the subsequent adsorption of thenaked anions on the surface of the copper anode and (iii) The oppositely directed migration of Cu^+ cations, and O^{2-} and S^{2-} anions, in the surface layer followed by the formation of reaction products. The similarity in sizes of the O^{2-} (~0.37 nm) and S^{2-} (~0.28 nm) with the length of the Cu-Cu bond in metallic copper (~0.36 nm) facilitates the diffusion of these anions into the metal lattice.[43] Therefore, in aqueous solutions, hydroxyl and oxide anions react with the copper anode to form Cu_2S, Cu_2O, $Cu(OH)_2$ and CuO.[45, 46] However, the XPS data collected from our samples immediately after the anodic synthesis of copper sulfide nanostructures indicates the absence of copper oxides, which is further confirmed by the XRD data. We believe that the inhibition of oxide formation is due to the adequately high concentration of sulfide, which leads to a near-exclusive adsorption of hydrosulfide ions on the copper anode. Furthermore, Cu_2S film growth, as reported,[44, 47] occurred at relatively low concentrations of sulfide employed in the electrolyte (~0.001-0.05 M) and was controlled by the diffusion of sulfide/hydrosulfide ions to the surface.

The diffusion-limitation is expected to be weaker in our case due to the use of 0.1 M aqueous Na_2S electrolyte. The anodization current (shown in Fig. S2 in Supporting Information) reaches a local maximum within the first 10 seconds of anodization due to the formation of Cu_2S nuclei. As surface copper sites are exhausted, the ionic current associated with Cu_2S formation decreases and as the nuclei coalesce into a film, the current component due to water electrolysis also drops due the lower electronic conductivity of Cu_2S compared to Cu. Nearly 60 seconds into the anodization process, the current decrease is arrested and a plateau is observed. This is indicative of a second nucleation process due to the migration of Cu^+ ions through the film outward from the anode towards the electrolyte and their subsequent reaction with hydrosulfide/sulfide species to form Cu_2S. Subsequently, the solid-state migration of Cu^+ ions becomes the rate-limiting step. Fig. 4d is a schematic of the mechanism of the growth of vertically oriented copper sulfide nanostructure arrays. As illustrated, the mechanism may be described by formation of Cu^+ species on the surface of copper substrate upon application of voltage, that diffuse out from the surface through the spontaneously formed aqueous copper sulfide layer, in a direction parallel to the applied electric field, and the reaction of Cu^+ with S^{2-} (present in the electrolyte) to form vertically aligned structures. The diffusivity of sulfur is six orders of magnitude lower than that of copper and hence only Cu^+ may be assumed to diffuse through copper sulfide.[48-50] In the anodization process, an electric field, the magnitude of which is proportional to the anodization voltage, is induced between copper anode and the cathode that enhances the diffusion rate of Cu^+ in the copper sulfide film. The diffusion coefficient[51-53] of Cu in copper sulfides is 10^4-10^5 cm^2s^{-1}. Fast Cu^+ diffusion coupled with high affinity between copper and sulfur is the cause of fast kinetics of the vertically aligned copper sulfide nanostructure growth. The Cu_2S formed at the Cu_2S and electrolyte interface precipitates in a direction parallel to the electric field and

perpendicular to the copper substrate leading to the formation of vertically oriented nanostructures.

The rapid field assisted diffusion of Cu^+ is followed by oxidation at the copper sulfide-electrolyte interface at the tips and also at the sides leading to branch-like structures. Eventually, the formation of copper sulfide at the tips and the sides is limited by the mass transport of sulfide and hydrosulfide ions from the bulk. The formation of dendrites is attributed to the concurrent existence of a high driving force for the formation of Cu_2S, coupled with a diffusion-limited step.[54] Thus higher applied voltages, which increase the driving force for the reaction and produce faster migration of the Cu^+ ions to the electrolyte interface, lead to dendritic structures. On the other hand, we attribute the development of nanowall structures to restricted growth of certain facets, either due to lower copper ion mobilities in the respective crystallographic directions or due to slightly lower reactivity. At higher voltages, the driving force for Cu^+ ion migration and Cu-S bonding are both greater, due to which the nanowalls transform into dendritic nanorods and nanoleaves. Similar behaviour is obtained for the anodization of Cu thin films on kapton substrates in sulfide-bearing aqueous electrolytes (Fig. S4, in the Supporting Information section). For comparison to the nanostructured films, planar films of copper sulfide are shown in Fig. S5.

Voltage serves as a driving force for field-assisted diffusion of copper. It is inferred from the experimental data that a voltage of 1.5 V is only sufficient for copper to diffuse out at a fast enough rate to the copper sulfide-electrolyte interface (shown in Fig. 4d) to form vertically oriented unbranched structures, such as nanowalls. The explanation of nanowall formation at lower voltages is attributable to a balance between transport (or diffusion) and reaction of copper

with sulfur to form copper sulfide. Voltage of 1.5 V is inadequate to create extraneous diffusive effects in order to form branches. At high voltages, however, branching out is generally observed, as with nanostructres formed at 3, 4 and 8 V. With increasing time the coalescence of copper sulfide nanostructured branches form rod-like projections, for which we assign the term, "branched" nanorods. This above mechanism is further confirmed by Fig S6 in the supporting information section, where vertical orientation and branch formation is observed to evolve with increase in anodization voltage. Temperature is another driving force that directly affects both transport and reaction kinetics. Given the high affinity between copper and sulfur, the low temperature of 5 °C, used in our growth process, served to retard the diffusive and reactive processes enabling more uniform nanostructure growth.

3.3 Structural analysis by XRD and TEM

Grazing incidence X-ray diffraction (GIXRD) patterns of the Cu_2S nanostructures formed at 1.5 V at room temperature, and 3 V at room-temperature and 5º C, are shown in Fig. 5. The GIXRD patterns of all samples in Fig. 5 show metallic copper peaks corresponding to the substrate. The diffractograms of samples anodized at 3 V at 5 ºC, and anodized at 1.5 V at room temperature, overlap perfectly as seen in Fig. 5. For both these overlapping patterns, the most intense peak not attributable to the substrate occurs at a 2-theta value of 45.99º. Considering that the strongest peak for monoclinic low chalcocite is the (630) reflection occurring at 45.98º, we matched the peaks with those of low chalcocite. The diffractogram showing the complete assignment of peaks to the low chalcocite pattern may be found in Fig. S3 in the supporting information section. However, the copper-deficient djurleite phase also possessing monoclinic symmetry, has several close-lying and overlapping peaks with low chalcocite. Furthermore, the phase field of low chalcocite extends to a Cu:S ratio of 1.991 on the sulfur-rich side while that of

djurleite exists between a Cu:S ratio of 1.934-1.965.[55] As K.E. Plass and colleagues have pointed out, distinguishing the monoclinic α-chalcocite phase (also known as low chalcocite) from djurleite is non-trivial.[56, 57] We closely compared peak positions and relative intensities of the low chalcocite and djurleite patterns with those of our samples. Our samples exhibit a cluster of four peaks from 35-40 degrees separated by approximately 1º as seen in Fig. 5. Djurleite has only one intense peak – the (434) reflection - in the 35-40º region whereas low chalcocite has several peaks of moderate to high intensity in the same region. The unique djurleite peak at 26.20º is entirely absent in our data. On the other hand, unique chalcocite peaks at 30.30º and 32.88º are indeed present as well as the peak at 40.80º, which is expected to be more prominent in chalcocite rather than djurleite. The changes in morphology are also accompanied by changes in phase and composition. Fig. 5 also shows that the sample anodized at room temperature at 3 V (black curve) exhibits a significantly different pattern from the other two samples; the differing pattern corresponds to the hexagonal Covellite phase (CuS), which is a stoichiometric compound with a very narrow phase field.[55]

GIXRD patterns of 3 V anodized sample, anodized for 15 seconds, 1 minute and 5 minutes are shown in Fig. S3. The phase is primary low chalcocite at 15 seconds and 1 minute whereas it is primary covellite at 5 minutes of anodization. Correlating with XRD data with SEM micrographs, it is evident that nanowall like structures are copper rich sulfides (i.e. low chalcocite), nanoleaves and rods containing nanobranches structures are relatively copper lean sulfides (i.e. covellite). Selected area electron diffraction (SAED) patterns obtained from TEM are shown in Figs. 6 and 7. The corresponding HRTEM lattice images are shown in Fig. S7. SAED patterns in Figs. 6a and 7b show a spot pattern due to the oriented crystallites while in Figs. 6b and 7a, SAED shows ring patterns due to the random orientation of crystallites and

mixed phase of the low chalcocite and CuS. In Fig. 6a, SAED patterns are indexed to (022), (450), (034) and (023) planes of the low chalcocite phase and lattice spacings are in agreement with JCPDS file 01-083-1462, which indicates the nanowalls formed by anodization at 5°C to be nearly exclusively Cu_2S. A mixture of Cu_2S and CuS is obtained for other anodization conditions. For higher anodization voltages and temperatures, the percentage of Cu_2S declines as the phase composition tends towards pure CuS.

There have been several recent reports on the syntheses of colloidal suspensions of Cu_2S nanoparticles. However, the majority of these papers form the high chalcocite phase bearing hexagonal symmetry. There is also a recent report on the synthesis of colloidal djurleite nanorods.[58] High chalcocite is copper deficient due to which it exhibits quasi-metallic behaviour. The generation of the monoclinic low chalcocite phase is more desirable from the point of view of exploiting the semiconducting properties of Cu_2S. However, there are only a few reports on the formation of low chalcocite nanostructures and iron stabilization is frequently used to achieve the same. There are a number of metastable phases in the Cu-S system with considerably different optoelectronic properties. For instance, our results demonstrate the possibility of phase selective synthesis of copper sulfide nanostructures by varying voltage, time and temperature during the electrochemical anodization of copper foils. Our results also show that anodization at low voltages and at low temperatures in aqueous solutions containing sulfide ions produces copper sulfide approaching phase-pure low chalcocite.

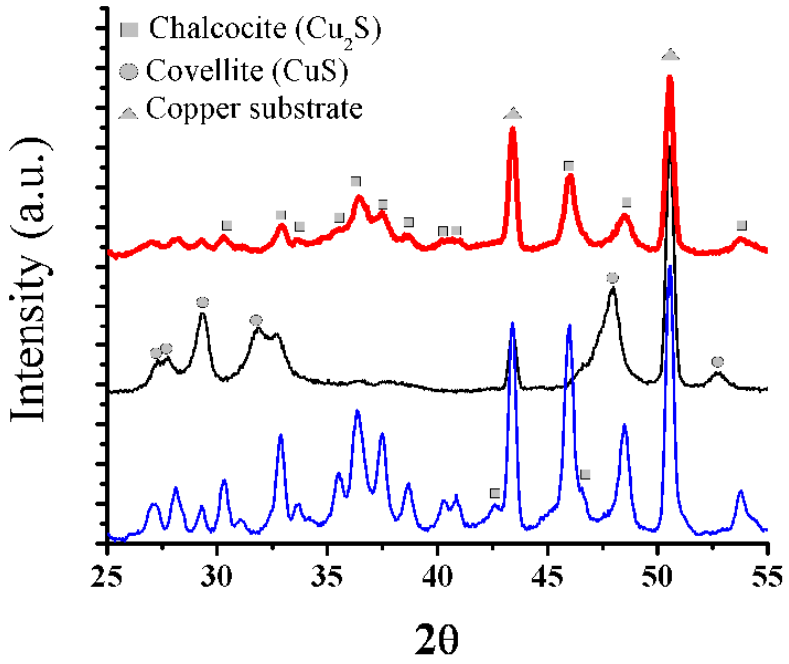

Fig. 5 Grazing incidence X-ray diffractograms of Cu foil samples subsequent to anodization. Three different diffractograms shown are 1.5 V at room temperature (red), 3 V at 5ºC (blue) and 3 V at room temperature (black). Peaks identified and as shown in the XRD patterns are those of Chalcocite (Cu_2S, JCPDS 01-0831462), Covellite (CuS, JCPDS 01-078-2121), and copper (due to copper substrate, JCPDS 01-0713761).

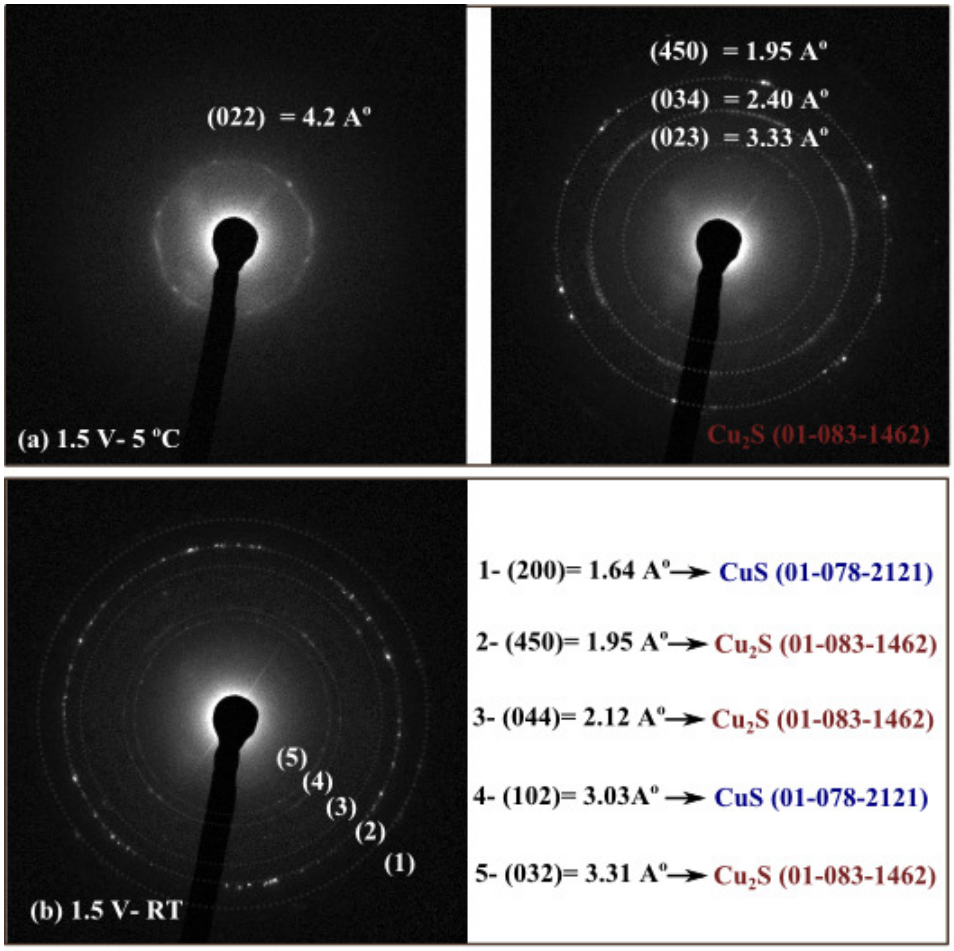

Fig. 6 Indexed electron diffraction patterns obtained from HRTEM of Cu foil samples anodized at 1.5 V at (a) 5°C and (b) Room temperature.

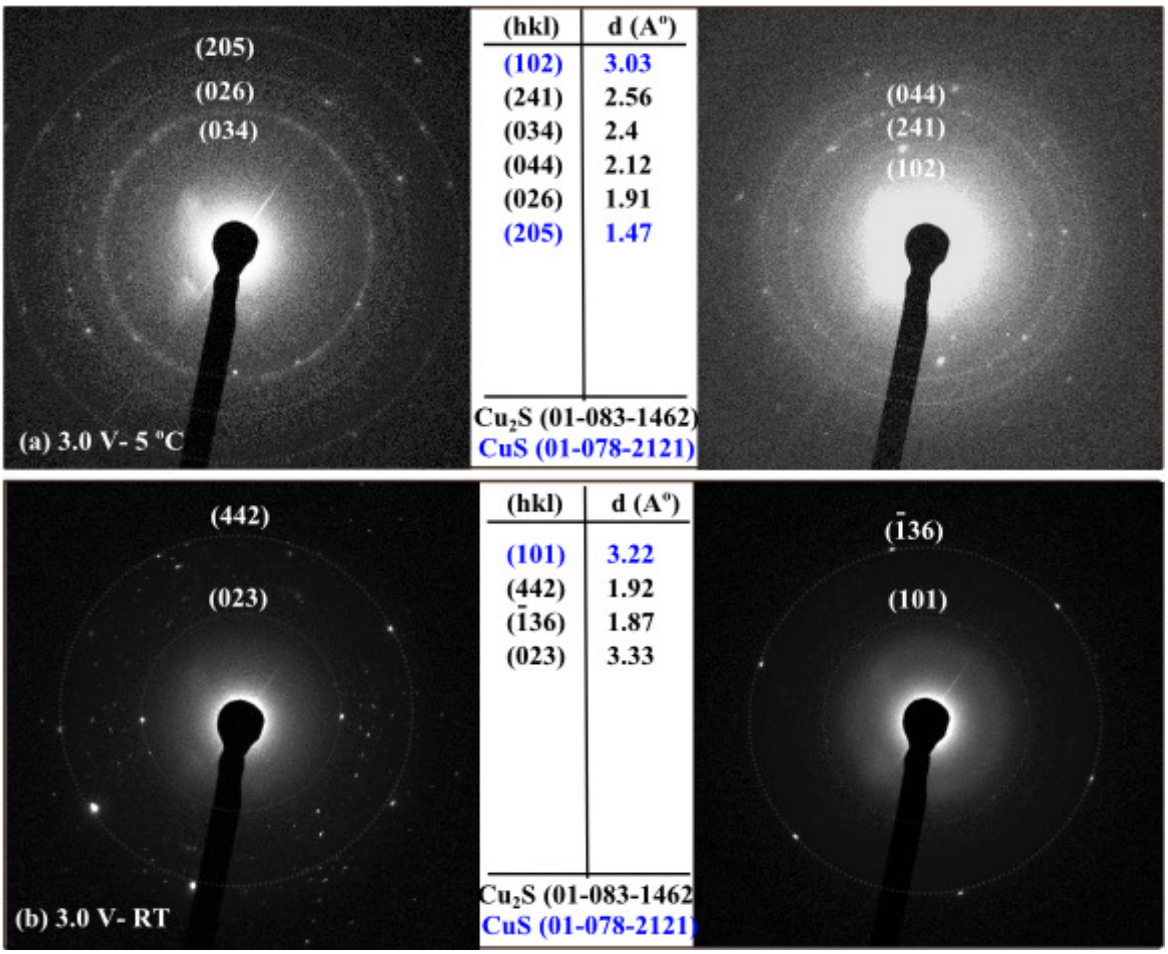

Fig. 7 Indexed electron diffraction patterns obtained from HRTEM of Cu foil samples anodized at 3 V at (a) 5°C and (b) Room temperature.

3.4 XPS analysis

While the XRD data derived from the 2-4 µm-thick anodized copper sulfide films are indicative of nearly pure phases of low chalcocite and covellite respectively, for the nanowall and nanorod arrays, high resolution X-ray photoelectron spectroscopy (XPS) data from the surface of the films, shown in Fig. 8**,** also suggests the presence of Cu_2S or CuS.[59-62] The S 2p peak (inset of Fig. 8) at 161.8 eV confirms the presence of Cu_2S while the peak at 162.8 eV is indicative of CuS wherein the binding energy of the S 2p photoelectron is at least 0.7 V higher

than in Cu_2S. The inset in Fig. 8 shows the S 2p peaks splitting into 2p3/2 and 2p1/2, with peak areas in the ratio of 2:1 (approximately). The split peaks are separated by about 1.2 eV (approximately), which is consistent with what is reported in many literature reports, for both, CuS and Cu_2S. It is also well-known that the surface of Cu_2S is oxidized in air due to which, samples indicated by XRD to be mostly α-chalcocite possibly exhibit S 2p peaks corresponding to CuS.[63] The S2p peak at 160.8 eV is Cu_2S as reported[64]. The Cu 2p spectra for the 1.5 V sample in Fig. 8 consist of the Cu $2p_{3/2}$ peak at 932.6 eV and the Cu $2p_{1/2}$ peak at 952.5 eV, which is as expected for Cu_2S. As the anodization voltage is increased from 1.5 V to 8 V, the corresponding peaks occur at slightly lower binding energies, as resolved by our instrument and are due to CuS.[63, 65]

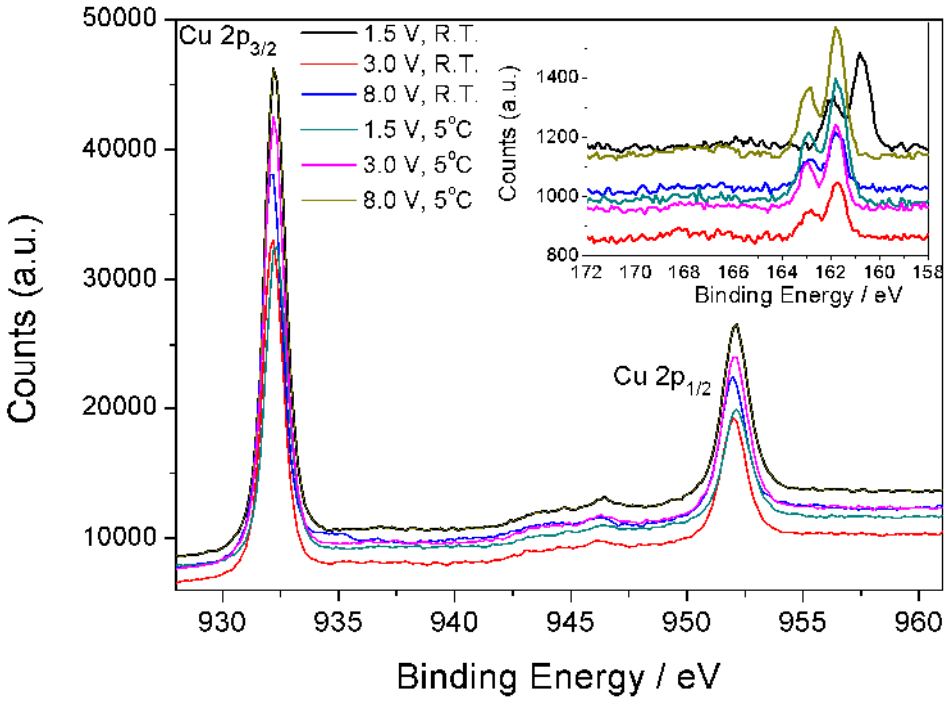

Fig. 8 XPS data for copper anodized at different voltages at 5°C and room temperature (R.T.), shows one set of peaks for Cu 2p3/2 between 932.3 and 932.5 eV and another set of peaks Cu 2p1/2 peaks that appear between 952.3 and 952.5 eV, confirm presence of Cu_2S and CuS.

3.5 EIS and Mott Schottky analysis

The copper sulfide-electrolyte interface was characterized by EIS and Mott Schottky analysis. Complex plane representation of the EIS data (i.e. Nyquist plots) along with fitted curves for 1.5 and 3.0 V anodized nanostructures are shown in Figs. 9b and c, respectively. The equivalent circuit used for fitting the EIS data is shown in Fig. 9a. Both, the Nyquist plot and the equivalent circuit resemble those for similar nanostructures as found in literature.[66-68]

The nanostructures clearly show two distinctive features in the Nyquist plots, which are characterized by a high frequency time constant connected to an intermediate to low frequency (i.e. 1 to 4000 Hz) pseudo-Warburg element. The equivalent circuit has an electrolyte resistance element, called $\boldsymbol{R_s}$. We associate the high frequency response to a time constant represented by a charge transfer resistance, $\boldsymbol{R_1}$, and a surface double layer capacitance, $\boldsymbol{C_1}$. Impedance magnitudes for resistances are frequency independent, for example the impedance of $\boldsymbol{R_1}$ is the same as $\boldsymbol{R_1}$. The impedance for $\boldsymbol{C_1}$ is given by:

$$Z_{C_1} = \frac{1}{i\omega C_1} \qquad \textbf{[1]}$$

In eqn. **[1]**, $\boldsymbol{i} = \sqrt{-1}$, $\boldsymbol{\omega}$ is the angular frequency and equals $\boldsymbol{2\pi f}$, where $\boldsymbol{f}$ is the frequency of applied alternating current (AC) signal. The intermediate to low frequency response was fitted to a series combination of a constant phase element (***CPE***) and a parallel connection comprising of a capacitance $\boldsymbol{C_2}$, and resistance, $\boldsymbol{R_2}$. The ***CPE*** is defined by $\boldsymbol{Q}$ with an exponent of $\boldsymbol{\alpha}$. $\boldsymbol{Q}$ is capacitive when $\boldsymbol{\alpha}$ is close to one, and resembles the Warburg element when $\boldsymbol{\alpha}$ is close to 0.5. The impedance for ***CPE*** and $\boldsymbol{C_2}$ are frequency dependent and are given by **[2]** and **[3]**.

$$Z_Q = \frac{1}{(i\omega)^{\alpha} Q} \qquad \textbf{[2]}$$

$$Z_{C_2} = \frac{1}{i\omega C_2} \qquad \textbf{[3]}$$

The total impedance of the impedance of the system, as illustrated by the equivalent circuit (Fig. 9a), is fitted to experimental data to extract the circuit parameters. For both copper sulfide nanostructures examined, values of $\boldsymbol{\alpha}$, as extracted from fitted data, are between 0.4 and 0.6, which suggests that the ***CPE*** corresponds to a generalized Warburg element, which occurs at low frequencies. Physically, this might imply a phenomenon like localized corrosion at low frequencies, which could be because of a variety of reasons, including exposure of small sections of copper foil (underneath the copper sulfide film) to the electrolyte. Physically, $\boldsymbol{C_2}$ may be attributed to space charge capacitance and $\boldsymbol{R_2}$ is the transport resistance. $\boldsymbol{C_2}$ is three to four orders of magnitude higher than $\boldsymbol{C_1}$. Charge carriers are copper vacancies in case of Cu_2S and sulfur vacancies in case of CuS, and their slow transfer to or from the semiconductor-electrolyte interfaces at intermediate to low frequencies justify the assignment of $\boldsymbol{C_2}$ to space charge capacitance. Electrical double layer formation is assumed to be in the copper sulfide nanostructure-electrolyte interface, while the space charge layer is assumed to form within the bulk of the films.

Conforming to the *p*-type characteristics of the nanostructures, Nyquist plots (Fig. 9b) evolve with applied potential, exhibiting an increase in the imaginary part of the impedance between the intermediate to low frequency as applied potential is made more negative, for Cu_2S nanowalls. A different behaviour is observed for *n*-type CuS samples in Fig. 9c (*n*-type character

of CuS nanostructures is shown in our Mott-Schottky analysis, later in this section). It follows from our EIS analysis that Cu_2S nanostructures have a $\boldsymbol{R_2}$ of 14 ohms and a $\boldsymbol{R_1}$ of 13 ohms, and also that CuS nanostructures have a $\boldsymbol{R_2}$ of 28 ohms and a $\boldsymbol{R_1}$ of 30 ohms. Values of $\boldsymbol{R_1}$ and $\boldsymbol{R_2}$ affect operational performance in photochemical and electrochemical devices.

Impedance is influenced by the defect distribution within the nanostructures formed on the underlying metal substrates. The point defect model by MacDonald implies exponential decrease of defect concentration[69] from the metal film interface, which however is not proven for sulfide films. So, we assume a uniform defect distribution, as required in classical Mott-Schottky analysis. Data for Mott-Schottky analysis was collected at room temperature for Cu_2S and CuS samples and is displayed in Figs. 9d–g. The frequency of the AC signal was 5 kHz and potential was varied between 0 and -1 V (w.r.t. Ag/AgCl). Plots of inverse squares of space charge capacitance versus potential gave the Mott-Schottky plots (Figs. 9 d, e, f and g). A roughness factor of 5 was assumed. Slopes (i.e. $\boldsymbol{m}$ in **[4]**) of straight line fits of the linear section of the data were used to calculate charge carrier concentration using **[4]**.

$$n = \frac{2}{e\varepsilon\varepsilon_0 m} \qquad \textbf{[4]}$$

Values of constants used in **[4]** are: $\boldsymbol{\varepsilon_0}$ = 8.854 187 817x 10^{-12} $F \cdot m^{-1}$ (vacuum permittivity); $\boldsymbol{\varepsilon}$ = 100 (dielectric constant for copper sulfide); $\boldsymbol{e}$ = 1.60217657 × 10^{-19} C (electron charge);

p-type conductance is observed from the Mott-Schottky plots for both 5°C and room temperature anodized Cu_2S nanostructures (formed at 1.5 V), and *n*-type conductance is observed for CuS nanostructures formed by anodization at 3V at 5 °C and room temperature.

While *p*-type conduction is generally accepted for Cu_2S, our finding of *n*-type conductance for anodized CuS nanostructures is also consistent with literature reports.[70-72] The Mott Schottky plots (Figs. 9d–g) give a carrier concentration of 4.70 x 10^{23} cm^{-3} for the 1.5 V and room temperature anodized Cu_2S nanostructures, 2.82 x 10^{21} cm^{-3} for 1.5 V and 5 °C anodized Cu_2S nanostructures, 2.09 x 10^{21} cm^{-3} for the 3.0 V and room temperature anodized CuS nanostructures, and 2.82 x 10^{22} cm^{-3} for the 3.0 V and 5 °C anodized CuS nanostructures. These charge carrier concentration values are in line with values reported for planar copper sulfide films.[73, 74]

At 1.5 V anodization voltage and room temperature, copper ions migrate slowly allowing excess of acceptor sulfur sites to exist and concominant copper vacancy defect sites to form in the bulk of the nanostructures. The low temperature phenomena however allow for a lower concentration of sulfur sites because of slower sulfur diffusion rates from the nanostructure-electrolyte interface. Such a condition enables lower concentration of excess sulfur in the nanostructure bulk leading to a lower concentration of bulk copper vacancy defects. Hence copper defects or *p*-type (i.e. acceptor) charge carriers are lower in low temperature anodized Cu_2S nanostructures than in the room temperature ones. The 3 V anodized CuS nanostructures exhibit *n*-type electronic conduction because of an excess of sulfur vacancies. The excess of sulfur vacancies are due to a preponderance of copper sites fostered by faster electric field assisted migration of copper cations into the nanostructure bulk from the copper - copper sulfide interface. Lower temperature inhibits sulfur diffusion and therefore higher *n*-type (donor) carrier concentration is observed for the 5 °C anodized CuS nanostructures.

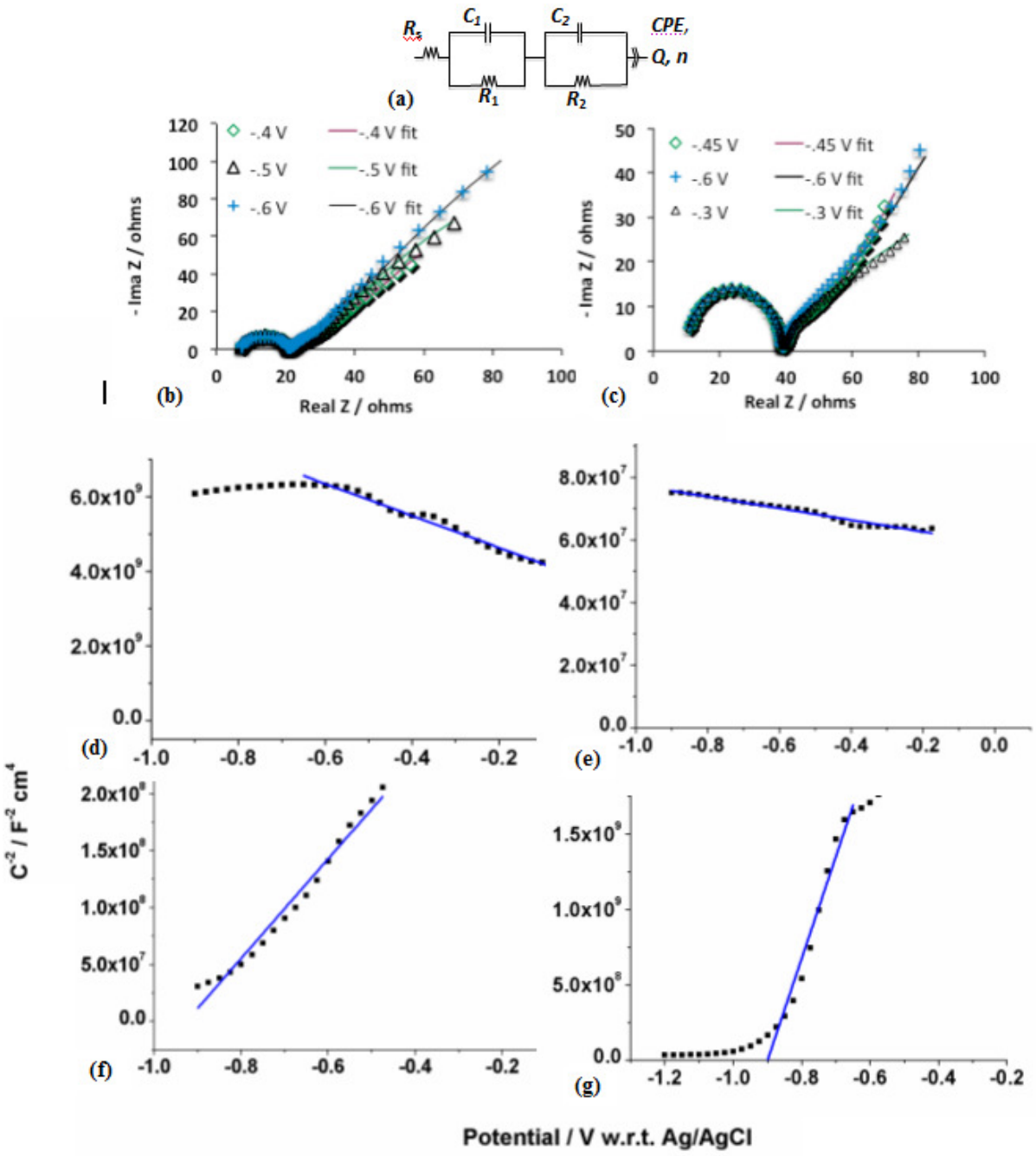

Fig. 9 (a) Equivalent circuit; (b) and (c) are Nyquist plots for 1.5 V and 3 V anodized copper sulfide nanostructures, respectively; (d) and (e) are Mott Schottky plots for Cu_2S nanowall arrays anodized at 5 ˚C and room temperature, respectively; (f) and (g) are Mott Schottky plots for CuS nanostructures anodized at 5 ˚C and room temperature, respectively; For (d), (e), (f) and (g), squares represent data and straight lines are linear fits from which slopes were extracted.

3.6 Photocatalytic CO_2 reduction with copper sulfide nanostructures

In our CO_2 reduction tests, reactor internal volume was 3 cm^2 and exposure duration of nanostructured copper sulfides to the incident simulated solar light was one hour. Schematic representation of the reactor used in our study is shown in Fig. 1. The photocatalytic reaction produced CH_4 by CO_2 reduction, the quantitative estimates of which, taken from at least three tests, are shown in Table 1 and representative GC spectra in Figs. S8 and S9 in the supporting information section. The CH_4 formation rate and quantity is low – indeed nearly two orders of magnitude smaller than today's best performing CO_2 reduction photocatalysts based on one-dimensional (1-D) TiO_2 nanostructures with co-catalyst promoters.[75, 76] But the significance is in this being the first such report using chalcogenides. The commonly cited reasons for skepticism of low numbers for CO_2 photoreduction, which lie in the possibility of carbon contamination, are not applicable here.[77] The cleaned copper foils were anodized in aqueous solutions of inorganic salts, rinsed in deionized water, dried in air and then used shortly after anodization in the reactors as stand-alone catalysts for CO_2 photoreduction. Organic solvents, organometallic precursors, self-assembled monolayers or organic compounds of any type were not used in the formation process, drastically minimizing the scope for carbon contamination. In view of the fast recombination due to the degenerate doping levels, the observed photocatalytic reaction yields are promising in this first study using copper sulfide nanostructures. CH_4 yield may be further improved by using co-catalyst promoters, wavelength and intensity of incident light, time of light exposure and also possibly temperature of the process. It is the authors' speculation that temperature needs to be optimized because elevated temperatures desorbs reaction products, activates reactions and improves diffusion of reactive species. The same tests, on non-nanostructured, planar films of Cu_2S (shown in Fig. S5 in Supporting Information) did not yield

any CH_4. The carrier concentration in copper sulfides is reported to reduce upon annealing in oxygen due to the formation of copper oxide species. Annealing our copper sulfide nanostructures in oxygen resulted in a complete loss of photocatalytic activity.

We examined band-structure and photocatalytic reaction pathways to explain why and how these copper sulfide nanostructures might be acting as stand-alone CO_2 photoreduction catalysts. *n*-type metal oxide semiconductors such as TiO_2 and WO_3 have been extensively studied as photocatalysts for both sunlight-driven water-splitting and sunlight-driven CO_2 reduction. However, the positions of the conduction band minima for both TiO_2 and WO_3 are more negative with respect to the vacuum level than the H^+/H_2 energy level (adjusted for over-potential) due to which transfer of photoelectrons from the CB of TiO_2/WO_3 to protons for hydrogen evolution is thermodynamically unfavourable. In practice, this necessitates the use of a co-catalyst such as Pd or Pt to reduce over-potentials and promote hydrogen evolution. Fig. 8 shows the band-diagrams of Cu_2S and CuS with respect to the relevant energy levels of the CO_2 photo-reduction reaction, which include the CO_2/CH_4 energy level at -0.24 eV and the over-potential adjusted energy levels for H_2 oxidation and O_2 evolution at -0.41 and +0.82 eV respectively. To construct these band-diagrams, electron affinities and band-gaps of Cu_2S and CuS were obtained from reports on high vacuum studies as well as studies of heterojunctions with CdS and other materials.[78] These values are expressed as a range in the band-diagram in recognition of the sensitivity of the electron affinities to the method of surface preparation and the prevailing ambient. Fig. 8 shows that the positions of the CB minimum and VB maximum in Cu_2S are favourable for CO_2 photo-reduction. This may explain the yields of methane, indicated in Table 1, in the absence of co-catalysts.

Sample type Anodization voltage, temperature (and time)	CH_4 yield, Average ± Std. deviation [μmole m^{-2} hr^{-1}]
1.5 V, 5 °C	46.21 ± 6.50
1.5 V, room temperature	39.42 ± 4.69
3 V, 5 °C	39.20 ± 11.55
3.0 V, room temperature, 4 minute	32.20 ± 3.26

Table 1. Photocatalytic performance of copper sulfide nanostructures formed by anodization Cu foil at various synthesis and testing conditions, inclusive of coating with nanoparticles of Cu, Pt, and together Cu and Pt . Numerical figures are averages of at least three readings. Tests were conducted for one hour at room temperature.

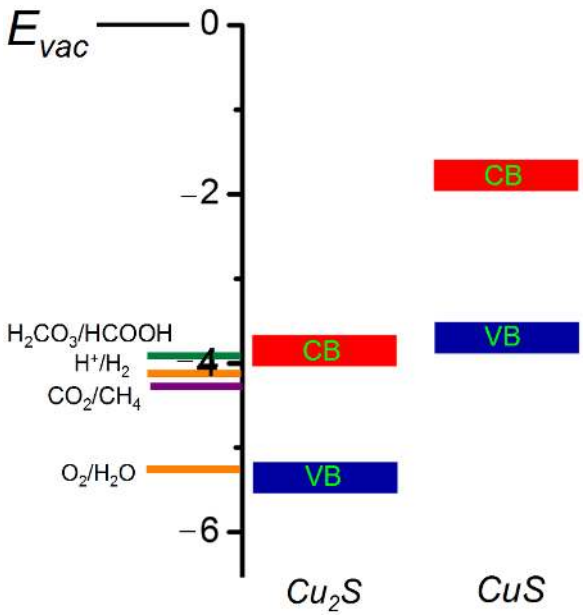

Fig. 10 Band-diagrams of Cu_2S and CuS in relation to the energy levels for water-splitting and CO_2 reduction.

For the formation of CH_4 (gas) with CO_2 (gas) and H_2O (vapour) precursors, the multi-step reaction mechanism is presumed to involve water splitting and hydrogen oxidation at the valence band edge followed by CO_2 reduction at the conduction band edge of the *p*-type Cu_2S. The water splitting reaction is given by:

$$H_2O \rightarrow H_2 + (\frac{1}{2})O_2 \qquad [5]$$

Electrochemically, the water oxidation is given by:

$$H_2O \rightarrow 2H^+ + 2e^- + (\frac{1}{2})O_2 \qquad [6]$$

The Gibbs free energy for water reduction at standard temperature and pressure is 2.46 eV, which equates to 1.23 eV per electron transfer. Thermodynamically, therefore the electron transfer for hydrogen oxidation requires the valence band edge of Cu_2S to be at least 1.23 eV negative with respect to the hydrogen oxidation potential.[79] The photo-reduction of CO_2 to methane involves eight electrons and four two-electron transfer reaction steps, as given below:

$$CO_2 + 2H^+ + 2e^- \rightarrow HCOOH \qquad [7]$$

$$HCOOH + 2H^+ + 2e^- \rightarrow HCHO + H_2O \qquad [8]$$

$$HCHO + 2H^+ + 2e^- \rightarrow CH_3OH \qquad [9]$$

$$CH_3OH + 2H^+ + 2e^- \rightarrow CH_4 + H_2O \qquad [10]$$

Energetics of all the four reactions (i.e. **[7], [8], [9] and [10]**) are thermodynamically feasible because the conduction band minimum of Cu_2S is favorably located at higher energy levels than the reduction potentials of CO_2, HCOOH, HCHO and CH_3OH. Typical values of reduction

potential for reactions given by [**7**] to [**10**] are between -4.76 and -4.46 eV with respect to vacuum at pH 5 in aqueous environment.[80]

More intriguing is the effect of anodization voltage for nanostructure formation on reaction yields because of the occurrence of both *p*-type and *n*-type carrier conductance in different types of nanostructures. XRD studies clearly indicate that at anodization voltages of 3 V and higher, and when the anodization was performed at room temperature, the covellite phase corresponding to CuS is dominant. CuS is reported to be a relatively poor stand-alone photocatalyst for water-splitting, a key intermediate step for CO_2 photoreduction. This is also evident from the EIS analysis presented earlier, where we report that Cu_2S nanowalls exhibit a lower (actually one-third) charge transfer resistance than CuS nanorods, supporting the observed phenomenon of higher photocatalytic activity with Cu_2S nanowalls, as compared to CuS nanorods. In addition, Mott-Schottky analysis revealed that the Cu_2S nanostructures have one order of magnitude higher charge carrier concentrations compared to the CuS nanostructures, which affects charge carrier recombination losses during photocatalysis.

This raises at least three possibilities: (i) Cu_2S impurities in covellite (CuS) shown in Fig. 7 assist in water-splitting, (ii) the phenomenon of CO_2 reduction reaction aided by the conversion of Cu_2S to CuS i.e. purely electrochemical reduction of CO_2 by Cu^+ and (iii) the reaction mechanism is unconventional. (i) is the more likely scenario given the smooth drop-off in CO_2 photoreduction yields and the fact that the S 2p XPS spectra (Fig. 8) show the lower BE peaks at 161.8 eV even for samples where XRD suggests covellite is the dominant phase; (ii) is unlikely considering the redox potentials for oxidation of Cu^+ in both aqueous media (-0.159 V vs. NHE) and in the solid-state (-0.05 V) are not conducive to the multi-step electron transfer reactions shown in Eqns. 7

through 10, and depicted in Fig. 10. However, (iii) cannot be ruled out since the high carrier density of copper sulfide enables plasmonic effects in photocatalysis[81] and there is also some support for positively charged quaternary ammonium ions suppressing hydrogen evolution, stabilizing intermediates in the CO_2 reduction process and reducing the relative over-potential for CO_2 reduction albeit aqueous media are typically required.[82] In this scenario, the high density of holes in Cu_2S may play an important role in the generation of protons from adsorbed water molecules and in inhibiting hydrogen evolution.

4 Conclusions

Vertically oriented copper sulfide nanowalls, nanoleafs and rods bearing three-dimensional (3D) dendritic nanobranches were formed by electrochemical anodization of copper foil and copper-coated Kapton substrates, in sodium sulfide electrolyte. These nanostructures are particularly interesting due to their vertical orientation and leaf-like or branched structure and hence enhanced structural intricacy coupled with their favourable functionality. Findings on the detailed characteristics of the nanostructures by using X-ray diffraction, elemental analysis by X-ray photoelectron spectroscopy and electronic properties by electrochemical impedance spectroscopy are reported. Anodization at 1.5 and 3 V, with temperature maintained at 5ºC, results in low chalcocite nanowall arrays that are curled at 1.5 V and straight at 3 V. Anodization at room temperature also results in curled nanowall arrays at 1.5 V. The 3 V anodization voltage at room temperature results low chalcocite nanowalls for short anodization times of 15 seconds and 1 minute. With a longer anodization time of 5 minutes, and voltage of 3 V, the low chalcocite nanowalls transform to covellite rods bearing dentritic nanobranches. Nanoleaf

morphology was obtained at 4 and 8 V by maintaining temperature at 5 ºC. XPS data confirms the presence of Cu_2S or CuS for both room temperature and 5 ºC anodized samples. Upon irradiation by AM 1.5 simulated sunlight, unoptimized anodically formed copper sulfide nanostructures showed promising photocatalytic performance, without any co-catalyst or promoter, in the conversion of CO_2 into CH_4. EIS and Mott Schottky analyses showed the *p*-type nature of the anodic Cu_2S and *n*-type nature of anodically formed CuS nanostructures and led to conclusive insights about the carrier concentrations.

Acknowledgements

This project was funded by the National Research Council of Canada and Alberta nanoBridge. S.F. was supported by a graduate student scholarship from Alberta Innovates Technology Futures. We acknowledge the assistance provided by Mr. Babak Amirsolaimani in measuring photocatalytic reaction products. Some device fabrication and testing used research infrastructure made possible by a Leaders Opportunity Fund grant to K.S. from the Canada Foundation for Innovation (CFI) and the Alberta Small Equipment Grants Program (SEGP). We acknowledge use of the following facilities: the NRC-NINT Electron Microscopy Lab (with special thanks to Drs. Kai Cui and Peng Li), the University of Alberta Nanofab and the Alberta Centre for Surface Engineering and Science (ACSES). We also thank Prof. Greg Dechaine and Weizhu An for assistance with GC setup and measurements, and Herbert Dexel for help with reactor design and fabrication.

References

1. Y. B. He, A. Polity, I. Österreicher, D. Pfisterer, R. Gregor, B. K. Meyer and M. Hardt, *Physica B: Condensed Matter*, 2001, 308–310, 1069-1073.
2. J. Y. Leong and J. H. Yee, *Applied Physics Letters*, 1979, 35, 601-602.
3. O. Madelung, *Semiconductors : Data Handbook*, Springer-Verlag, 2004.
4. M. Page, O. Niitsoo, Y. Itzhaik, D. Cahen and G. Hodes, *Energy & Environmental Science*, 2009, 2, 220.
5. A. Rothwarf and H. Windawi, *Electron Devices, IEEE Transactions on*, 1981, 28, 64-69.
6. A. C. Rastogi and S. Salkalachen, *Thin Solid Films*, 1982, 97, 191-199.
7. Y. Zhao and C. Burda, *Energy & Environmental Science*, 2012, 5, 5564-5576.
8. P. Lukashev, W. R. L. Lambrecht, T. Kotani and M. van Schilfgaarde, *Physical Review B*, 2007, 76, 195202-195201-195202-195214.
9. Q. Xu, B. Huang, Y. Zhao, Y. Yan, R. Noufi and S.-H. Wei, *Applied Physics Letters*, 2012, 100, 061906-061906-061904.
10. Y. X. Zhao, H. C. Pan, Y. B. Lou, X. F. Qiu, J. J. Zhu and C. Burda, *Journal of the American Chemical Society*, 2009, 131, 4253-4261.
11. I. Kriegel, C. Jiang, J. Rodríguez-Fernández, R. D. Schaller, D. V. Talapin, E. da Como and J. Feldmann, *Journal of the American Chemical Society*, 2011, 134, 1583-1590.
12. W. Liang and M. H. Whangbo, *Solid State Communications*, 1993, 85, 405-408.
13. H. Nozaki, K. Shibata and N. Ohhashi, *Journal of Solid State Chemistry*, 1991, 91, 306-311.
14. M. Lee and K. Yong, *Nanotechnology*, 2012, 23.
15. J. Zhang, J. G. Yu, Y. M. Zhang, Q. Li and J. R. Gong, *Nano Lett.*, 2011, 11, 4774-4779.
16. R. R. Gainov, A. V. Dooglav, I. N. Pen'kov, I. R. Mukhamedshin, N. N. Mozgova, I. A. Evlampiev and I. A. Bryzgalov, *Physical Review B*, 2009, 79, 075115-075111-075115-075111.
17. I. I. Mazin, *Physical Review B*, 2012, 85, 115133-115131-115133-115135.
18. H. C. Hadley and W. F. Tseng, *Journal of Crystal Growth*, 1977, 39, 61-72.
19. F. A. Shirland, *Journal of Applied Physics*, 1979, 50, 4714-4719.
20. Y. Wu, C. Wadia, W. L. Ma, B. Sadtler and A. P. Alivisatos, *Nano Letters*, 2008, 8, 2551-2555.
21. M. Peng, L. L. Ma, Y. G. Zhang, M. Tan, J. B. Wang and Y. Yu, *Materials Research Bulletin*, 2009, 44, 1834-1841.
22. J. Chen, S. Z. Deng, N. S. Xu, S. H. Wang, X. G. Wen, S. H. Yang, C. L. Yang, J. N. Wang and W. K. Ge, *Applied Physics Letters*, 2002, 80, 3620-3622.
23. T. Sakamoto, H. Sunamura, H. Kawaura, T. Hasegawa, T. Nakayama and M. Aono, *Applied Physics Letters*, 2003, 82, 3032-3034.
24. M. Xu, L. Cui, R. Han and S. Ai, *Journal of Solid State Electrochemistry*, 2012, 16, 2547-2554.
25. X. L. Yu, C. B. Cao, H. S. Zhu, Q. S. Li, C. L. Liu and Q. H. Gong, *Advanced Functional Materials*, 2007, 17, 1397-1401.
26. Q. W. Tian, M. H. Tang, Y. G. Sun, R. J. Zou, Z. G. Chen, M. F. Zhu, S. P. Yang, J. L. Wang, J. H. Wang and J. Q. Hu, *Advanced Materials*, 2011, 23, 3542-3547.
27. R. Cai, J. Chen, J. X. Zhu, C. Xu, W. Y. Zhang, C. M. Zhang, W. H. Shi, H. T. Tan, D. Yang, H. H. Hng, T. M. Lim and Q. Y. Yan, *Journal of Physical Chemistry C*, 2012, 116, 12468-12474.
28. C. H. Lai, K. W. Huang, J. H. Cheng, C. Y. Lee, B. J. Hwang and L. J. Chen, *Journal of Materials Chemistry*, 2010, 20, 6638-6645.
29. K.-S. Choi, H. S. Jang, C. M. McShane, C. G. Read and J. A. Seabold, *MRS Bulletin*, 2010, 35, 753-760.

30. B. J. Mulder, *physica status solidi (a)*, 1972, 13, 569-575.
31. M. A. Rafea, A. A. M. Farag and N. Roushdy, *Materials Research Bulletin*, 2012, 47, 257-266.
32. J. Johansson, J. Kostamo, M. Karppinen and L. Niinisto, *Journal of Materials Chemistry*, 2002, 12, 1022-1026.
33. K. Anuar, Z. Zainal, M. Z. Hussein, N. Saravanan and I. Haslina, *Sol. Energy Mater. Sol. Cells*, 2002, 73, 351-365.
34. S. D. Sartale and C. D. Lokhande, *Mater. Chem. Phys.*, 2000, 65, 63-67.
35. A. Ghahremaninezhad, E. Asselin and D. G. Dixon, *Journal of Physical Chemistry C*, 2011, 115, 9320-9334.
36. Q. B. Wu, S. Ren, S. Z. Deng, J. Chen and N. S. Xu, *Journal of Vacuum Science & Technology B*, 2004, 22, 1282-1285.
37. G. Z. Mao, W. F. Dong, D. G. Kurth and H. Mohwald, *Nano Letters*, 2004, 4, 249-252.
38. K. V. Singh, A. A. Martinez-Morales, G. T. S. Andavan, K. N. Bozhilov and M. Ozkan, *Chemistry of Materials*, 2007, 19, 2446-2454.
39. L. Chen, Y. B. Chen and L. M. Wu, *Journal of the American Chemical Society*, 2004, 126, 16334-16335.
40. Q. Y. Lu, F. Gao and D. Y. Zhao, *Nano Letters*, 2002, 2, 725-728.
41. M. B. Sigman, A. Ghezelbash, T. Hanrath, A. E. Saunders, F. Lee and B. A. Korgel, *Journal of the American Chemical Society*, 2003, 125, 16050-16057.
42. Y. Linga, M. Taylora, S. Sharifiasla and D. Macdonald, *ECS Transactions*, 2013, 50, 53-67.
43. A. G. Makarov, V. V. Batrakov, G. V. Makarov and I. G. Gorichev, *Protection of Metals*, 2004, 40, 49-55.
44. M. I. Schimmel, O. L. Bottechia and H. Wendt, *Journal of Applied Electrochemistry*, 1998, 28, 299-304.
45. M. R. G. Dechialvo and A. J. Arvia, *Journal of Applied Electrochemistry*, 1985, 15, 685-696.
46. B. Scharifker, R. Rugeles and J. Mozota, *Electrochimica Acta*, 1984, 29, 261-266.
47. J. Chen, Z. Qin and D. Shoesmith, *J. Electrochem. Soc.*, 2010, 157, C338-C345.
48. R. Blachnik and A. Müller, *Thermochimica Acta*, 2000, 361, 31-52.
49. S. G. Tereshkova, *Kinetics and mechanism of copper interaction with gaseous sulfur*, Maik Nauka/Interperiodica, Moscow, Russie Federation De 1998.
50. F. Moya, G. E. Moya-Gontier, F. Cabane-Brouty and J. Oudar, *Acta Metallurgica*, 1971, 19, 1189-1194.
51. I. Bartkowicz and A. Stoklosa, *Oxid. Met.*, 1986, 25, 305-318.
52. S. Cassaignon, T. Pauporte, J. F. Guillemoles and J. Vedel, *Ionics*, 1998, 4, 364-371.
53. T. Pauporte and J. Vedel, *Solid State Ion.*, 1999, 116, 311-320.
54. H. Imai and Y. Oaki, *MRS Bulletin*, 2010, 35, 138-144.
55. D. Chakrabarti and D. Laughlin, *Journal of Phase Equilibria*, 1983, 4, 254-271.
56. M. Lotfipour, T. Machani, D. P. Rossi and K. E. Plass, *Chemistry of Materials*, 2011, 23, 3032-3038.
57. T. Machani, D. P. Rossi, B. J. Golden, E. C. Jones, M. Lotfipour and K. E. Plass, *Chemistry of Materials*, 2011, 23, 5491-5495.
58. M. Kruszynska, H. Borchert, A. Bachmatiuk, M. H. Rümmeli, B. Büchner, J. Parisi and J. Kolny-Olesiak, *ACS Nano*, 2012, 6, 5889-5896.
59. J. C. Klein, A. Proctor, D. M. Hercules and J. F. Black, *Analytical Chemistry*, 1983, 55, 2055-2059.
60. I. Nakai, Y. Sugitani, K. Nagashima and Y. Niwa, *Journal of Inorganic and Nuclear Chemistry*, 1978, 40, 789-791.
61. V. I. Nefedov, Y. V. Salyn, P. M. Solozhenkin and G. Y. Pulatov, *Surface and Interface Analysis*, 1980, 2, 170-172.

62. D. L. Perry and J. A. Taylor, *Journal of Materials Science Letters*, 1986, 5, 384-386.
63. S. K. Chawla, N. Sankarraman and J. H. Payer, *J. Electron Spectrosc. Relat. Phenom.*, 1992, 61, 1-18.
64. T. R. N. Kutty, *Materials Research Bulletin*, 1991, 26, 399-406.
65. V. Krylova and A. Andrulevicius, *Int. J. Photoenergy*, 2009.
66. J. M. Smith, J. C. Wren, M. Odziemkowski and D. W. Shoesmith, *Journal of The Electrochemical Society*, 2007, 154, C431 - C438.
67. W. Zhao, T. Lin, S. Sun, H. Bi, P. Chen, D. Wan and F. Huang, *Journal of Materials Chemistry A*, 2013, 1.
68. J. Zhu, Y. K. Sharma, Z. Zeng, X. Zhang, M. Srinivasan, S. Mhaisalkar, H. Zhang, H. H. Hng and Y. Qingyu, *The Journal of Physical Chemistry C*, 2011, 115, 8400 - 8406.
69. D. D. MacDonald, *Journal of The Electrochemical Society*, 1992, 139, 3434 - 3449.
70. Y. Ling, M. Taylor, S. Sharifiasl and D. Macdonald, *ECS Transactions*, 2013, 50, 53-67.
71. K. M. Rosso and M. F. Hochella Jr, *Surface Science*, 1999, 423, 364-374.
72. J. George and K. S. Joseph, *Solid State Communications*, 1983, 48, 601-603.
73. W. Liang and M. H. Whangbo, *Solid State Communications*, 1993, 85, 405-408.
74. R. R. Chamberlin and J. S. Skarman, *Solid State Electronics (Permangon Press)*, 1966, 9, 819-823.
75. W.-N. Wang, W.-J. An, B. Ramalingam, S. Mukherjee, D. M. Niedzwiedzki, S. Gangopadhyay and P. Biswas, *Journal of the American Chemical Society*, 2012, 134, 11276-11281.
76. X. Zhang, F. Han, B. Shi, S. F. Farsinezhad, G. P. Dechaine and K. Shankar, *Angewandte Chemie*, 2012.
77. C.-C. Yang, Y.-H. Yu, B. van der Linden, J. C. S. Wu and G. Mul, *Journal of the American Chemical Society*, 2010, 132, 8398-8406.
78. T. M. Razykov and B. K. Kadirov, *physica status solidi (a)*, 1984, 84, K71-K74.
79. L. A. Harris and R. H. Wilson, *Annual review of materials science*, 1978, 8, 99-134.
80. T. Inoue, A. Fujishima, S. Konishi and K. Honda, *Nature*, 1979, 277, 637-638.
81. W. Hou, W. H. Hung, P. Pavaskar, A. Goeppert, M. Aykol and S. B. Cronin, *ACS Catalysis*, 2011, 1, 929-936.
82. W. Zhu, B. Rosen and R. Masel, *Meeting Abstracts*, 2010, MA2010-02, 466.